

Additive Higher-Order Factorization Machines

David Rügamer
Institute of Statistics, RWTH Aachen
Department of Statistics, LMU Munich

Abstract

In the age of big data and interpretable machine learning, approaches need to work at scale and at the same time allow for a clear mathematical understanding of the method's inner workings. While there exist inherently interpretable semi-parametric regression techniques for large-scale applications to account for non-linearity in the data, their model complexity is still often restricted. One of the main limitations are missing interactions in these models, which are not included for the sake of better interpretability, but also due to untenable computational costs. To address this shortcoming, we derive a scalable high-order tensor product spline model using a factorization approach. Our method allows to include all (higher-order) interactions of non-linear feature effects while having computational costs proportional to a model without interactions. We prove both theoretically and empirically that our methods scales notably better than existing approaches, derive meaningful penalization schemes and also discuss further theoretical aspects. We finally investigate predictive and estimation performance both with synthetic and real data.

Keywords: Tensor-Product Splines, Scalability, Higher-Order Interactions

1 Introduction

Two of the core principles of statistical regression models are additivity and linearity of the predictors. These properties allow estimated feature effects to be easily interpreted, which also led to (revived) interest in such models in the machine learning community (Liu et al., 2008; Shan and Banerjee, 2010; Yin et al., 2012; Zhang et al., 2016; Chen et al., 2017; Pan et al., 2020; Wang et al., 2020; Zhuang et al., 2021; Chang et al., 2021). A frequently used and cited example of an interpretable yet flexible statistical regression model is the generalized additive model (GAM; Hastie and Tibshirani, 2017; Wood, 2017). Using basis functions to approximate non-linear functions, these models can represent non-linear feature effects in one or a moderate number of dimensions. Applying this principle in settings with many features and higher-order interactions, however, comes with considerable downsides. For univariate non-linear effects, the number of basis functions M for each feature typically lies in the range of 10 to 20 and needs to be evaluated prior to model fitting. Representing and fitting all available features using basis functions will not only result in a notable increase in training time, but also requires a considerable amount of additional memory. In higher dimensions D , these problems carry even more weight as D -variate non-linear representations are typically constructed using Kronecker or tensor product splines (TPS), i.e., a (row-wise) Kronecker product of all involved bases. This results in computational costs of $\mathcal{O}((pM)^D)$ for TPS models with p features. Computational feasibility is thus one of the main reasons statistical applications are often restricted to only uni- and bivariate (tensor product) splines. While several approaches to tackle this problem have been proposed (e.g., Wood et al., 2017), existing solutions still either suffer from extensive memory or runtime costs.

Our Contribution In order to efficiently scale additive models in higher dimensions (cf. also Figure 1), we propose an approach for modeling high-order TPS with linear complexity in D based on the idea of factorization machines (FMs; Rendle, 2010). While this effectively addresses existing scaling problems of GAMs, our approach also extends (higher-order) factorization machines by allowing for non-linear relationships. In addition to deriving

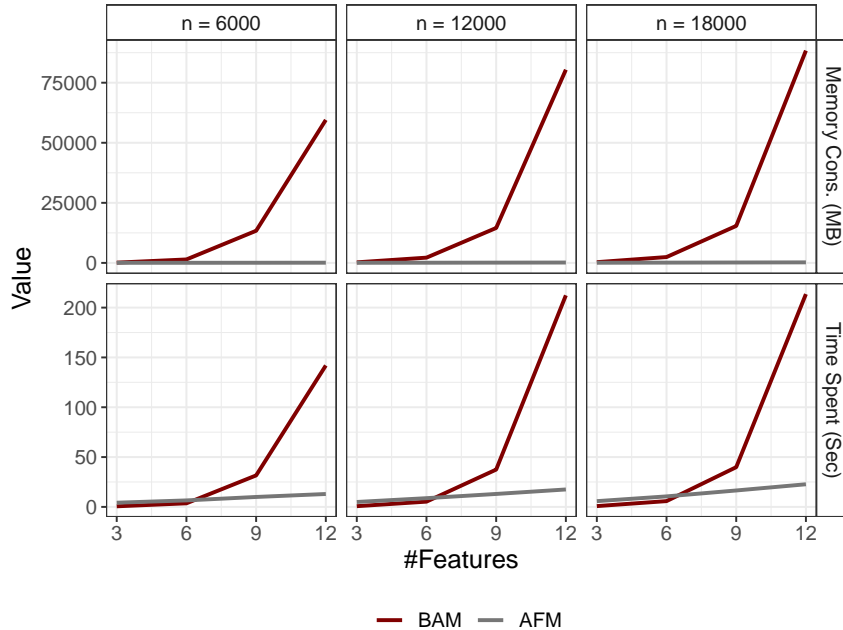


Figure 1: Comparison of memory consumption (first row) and time consumption (second row) between the state-of-the-art big additive model (BAM) implementation (in red) and our proposal (in gray) when fitting a model for all $\binom{p}{2}$ tensor product splines using different numbers of features p (x-axis) and observations (columns).

the resulting computational complexity, we also propose an efficient way of computing the model, suggest a suitable penalization scheme and provide an optimization routine for our approach. Our experimental section demonstrates that models with high-order TPS work well in practice and yield competitive results in comparison to other commonly used machine learning models.

2 Related Literature

Generalized Additive Models and Tensor-Product Splines GAMs extend generalized linear models (Nelder and Wedderburn, 1972) by allowing feature effects to be non-linear, typically achieved by using a spline bases representation. Next to basic principles (see, e.g., Hastie and Tibshirani, 2017; Wood, 2017), many extensions of GAMs have been discussed in the literature. In order to include non-linear functions of more than one variable, various

options exist, e.g., by using spline bases in multiple dimensions. Wood (2006) proposed a flexible way of constructing multivariate non-linear functions in GAMs using TPS as an alternative option, which we will outline in more detail in Section 3.2.2. Although GAM software is usually optimized in terms of efficiency, computational costs can be a bottleneck for large data sets or complex model formulations. While there exist approaches that allow GAM estimation for data with many observations (Wood et al., 2017), GAMs still scale unfavorably with many features or feature interactions. Recent approaches (Rügamer et al., 2020) suggest to fit structured regression models as (part of) a neural network. This can result in a better space complexity in situations with many data points and allows for more flexibility in the additive predictors of models beyond those of classical GAMs (see, e.g., Baumann et al., 2021; Kopper et al., 2021).

Factorization Approaches Similar to GAMs, factorization approaches have been studied extensively. Popularized for recommender systems, different (matrix) factorization approaches have been proposed in the early 2000s (see, e.g., Srebro et al., 2004; Adomavicius and Tuzhilin, 2005; Koren et al., 2009) and are still considered state-of-the-art in terms of performance and efficiency (Rendle et al., 2020; Jin et al., 2021). Closely related to matrix factorization are factorization machines (FMs; Rendle, 2010). FMs are based on a linear model formulation with pairwise interactions between all features and use a factorization trick to overcome unfavorable scaling when the number of features is large. Various extensions have been developed over the past years, including convex FMs (Blondel et al., 2015) and an efficient calculation of higher-order FMs (HOFMs; Blondel et al., 2016). Other extensions include boosted FMs (Yuan et al., 2017), FMs with special personalized feature treatment (Chen et al., 2019) or interaction-aware FMs (Hong et al., 2019). Similar to our proposal, Lan and Geng (2019) use a non-parametric subspace feature mapping to encode interactions and account for non-linearity, but rely on binning the features in grid cells.

Another related field that also uses factorization and low-rank assumptions is tensor regression (Zhou et al., 2013). In tensor regression features and/or outcome are assumed to be tensors and usually modeled by some type of factorization or low-rank assumption. Next to a concise representation, framing factorization approaches as linear tensor regression

theory allows to derive important theoretical concepts such as the Eckart-Young theorem (Eckart and Young, 1936). Several extensions to non-linear relationships exist. For example, a parametric non-linear factorization model was proposed recently by Zhang et al. (2021) for a tensor-shaped outcome variable that varies over time. In Blondel et al. (2016), a connection was made between HOFMs and a lifted (tensor) approach (Candes et al., 2015) to efficiently represent and compute HOFMs.

3 Background

We first introduce our notation in Section 3.1 and then give a short introduction into GAMs in Section 3.2. For more details, see, e.g., Wood (2017).

3.1 Notation

In the following, we write scalar values in small or capital letters without formatting, vectors in small bold letters, matrices in capital bold letters, and tensors using fraktur typeface, e.g., \mathfrak{X} . Calligraphic letters will have different meaning depending on the context, while \mathcal{O} is reserved to describe the complexity of calculations in terms of computing time or memory. The Mode-1 fiber of a three-dimensional tensor $\mathfrak{X} \in \mathbb{R}^{p_1 \times p_2 \times p_3}$ denotes the vectors obtained when fixing the second and third dimension of \mathfrak{X} to certain values i, j , i.e., $\mathfrak{X}_{:,i,j} \in \mathbb{R}^{p_1}$. Similar, $\mathfrak{X}_{:,:,j} \in \mathbb{R}^{p_1 \times p_2}$ are the frontal slices of \mathfrak{X} . For better readability, we will denote the sequence from $1, \dots, x$ with $[x]$. We further use \otimes for the Kronecker product. For two square matrices \mathbf{A}, \mathbf{B} with dimensions a and b , respectively, we define the *Kronecker sum* as $\mathbf{A} \oplus \mathbf{B} = \mathbf{A} \otimes \mathbf{I}_b + \mathbf{I}_a \otimes \mathbf{B}$, where \mathbf{I}_x is the identity matrix of dimension x . $\text{vec}(\cdot)$ denotes the vectorization operator to flatten a matrix or tensor along its dimensions.

3.2 Generalized Additive Models

Given the response random variable Y and p features $\mathbf{x} = (x_1, \dots, x_p)$, an additive model with linear and non-linear effects for all features assumes the following relationship:

$$Y = \eta(\mathbf{x}) + \varepsilon = \alpha_0 + \sum_{j=1}^p x_j \alpha_j + \sum_{j=1}^p f_j(x_j) + \varepsilon, \quad (1)$$

where $\alpha_0, \alpha_1, \dots, \alpha_p$ are linear regression coefficients, f_1, \dots, f_p univariate non-linear functions, $\varepsilon \sim \mathcal{N}(0, \sigma^2)$ is a zero-mean Gaussian random variable with variance $\sigma^2 > 0$ and η the model predictor. GAMs, the generalization of additive models, replace the distribution assumption in (1) using a more general distribution by assuming that $Y|\mathbf{x}$ has some exponential family distribution and $\mathbb{E}(Y|\mathbf{x}) = h(\eta(\mathbf{x}))$ for some monotonic (response) function h . A prediction $\hat{y} = h(\hat{\eta}(\mathbf{x}))$ for the observed value y in GAMs is formed by estimating the regression coefficients and functions f_j . GAMs can be optimized using (different types of) maximum likelihood estimation. Alternatively, using the negative log-likelihood as (convex) loss function ℓ , their optimization can also be framed as an empirical risk minimization problem.

Since linear effects α_j can be incorporated in the functions f_j , we will drop the linear model part in the following. The non-linear functions f_j in GAMs are usually approximated using a (spline) basis representation, i.e.,

$$f_j(x_j) \approx \sum_{m=1}^{M_j} B_{m,j}(x_j) \beta_{m,j} = \mathbf{B}_j^\top \boldsymbol{\beta}_j, \quad (2)$$

where $B_{m,j}$ are pre-defined basis functions (e.g., truncated polynomials or B-splines) and $\beta_{m,j}$ the corresponding basis coefficients. In the following, we summarize all basis functions and coefficients using $\mathbf{B}_j = (B_{1,j}, \dots, B_{M_j,j}) \in \mathbb{R}^{M_j}$ and $\boldsymbol{\beta}_j = (\beta_{1,j}, \dots, \beta_{M_j,j})^\top \in \mathbb{R}^{M_j}$, respectively. To enforce smoothness of the functions f_j , the $\boldsymbol{\beta}_j$ coefficients are typically estimated using a smoothness penalty.

3.2.1 Smoothness Penalties

One of the most common approaches to estimate smooth functions f_j is to employ a difference penalty for successive basis coefficients $\beta_{m,j}, \beta_{m+1,j}$ of basis functions $B_{m,j}(x), B_{m+1,j}(x)$,

which penalizes deviating behavior in neighboring basis functions. The penalty term for the penalized loss function is then given by

$$\mathcal{P} = \sum_{j=1}^p \lambda_j \int (f_j''(x))^2 dx,$$

which is a trade-off between goodness-of-fit and roughness of the functions f_j . The penalized loss can be written as

$$\ell(y, \hat{y}) + \sum_{j=1}^p \lambda_j \boldsymbol{\beta}_j^\top \mathbf{P}_j \boldsymbol{\beta}_j, \quad (3)$$

where $\mathbf{P}_j \in \mathbb{R}^{M_j \times M_j}$ is a squared penalty matrix depending on the evaluated basis \mathbf{B}_j for the j th feature and usually penalizes first or second differences in the coefficients $\boldsymbol{\beta}_j$.

GAMs also allow for higher dimensional non-linear functions, e.g., bivariate smooth terms $f_{k,l}(x_k, x_l)$. A common approach for their construction are tensor product splines.

3.2.2 Tensor Product Splines

While there are various approaches to construct smooth functions of several features, tensor product splines (TPS) constructed from marginal univariate bases constitute an attractive option. The resulting smooth terms are very flexible, scale-invariant, relatively low rank as well as easy to construct and interpret (see Wood, 2006). For a model with all $\binom{p}{2}$ possible bivariate effects, the TPS part is given by

$$\sum_{k=1}^p \sum_{l=k+1}^p f_{k,l}(x_k, x_l) \approx \sum_{k=1}^p \sum_{l=k+1}^p (\mathbf{B}_k \otimes \mathbf{B}_l) \boldsymbol{\beta}_{k,l} = \sum_{k=1}^p \sum_{l=k+1}^p \sum_{m=1}^{M_k} \sum_{o=1}^{O_l} B_{m,k}(x_k) B_{o,l}(x_l) \beta_{m,k,o,l} \quad (4)$$

with univariate spline basis functions $B_{m,k}$, $B_{o,l}$ and basis coefficients $\beta_{m,k,o,l}$, summarized in $\boldsymbol{\beta}_{k,l} \in \mathbb{R}^{M_k O_l}$. Bivariate TPS are penalized using

$$\mathcal{P}(f_{k,l}) = \int_{x_k, x_l} \lambda_k (\partial^2 f / \partial x_k^2)^2 + \lambda_l (\partial^2 f / \partial x_l^2)^2 dx_k x_l, \quad (5)$$

which can be written as

$$\mathcal{P}(f_{k,l}) = \boldsymbol{\beta}_{k,l}^\top (\lambda_k \mathbf{P}_k \oplus \lambda_l \mathbf{P}_l) \boldsymbol{\beta}_{k,l}. \quad (6)$$

This principle can be generalized to D -variate smooths for variables $\mathcal{J} := \{j_1, \dots, j_D\}$, which are approximated by

$$f_{j_1, \dots, j_D}(x_{j_1}, \dots, x_{j_D}) \approx (\otimes_{j \in \mathcal{J}} \mathbf{B}_j) \boldsymbol{\beta}_{\mathcal{J}}, \quad (7)$$

where $\boldsymbol{\beta}_{\mathcal{J}} \in \mathbb{R}^{\prod_{t=1}^D M_{j_t}}$ contains the coefficients for all combinations of the D basis functions. The corresponding penalty term for (7) is constructed analogously to (6) by $\boldsymbol{\beta}_{\mathcal{J}}^\top (\oplus_{j \in \mathcal{J}} \lambda_j \mathbf{P}_j) \boldsymbol{\beta}_{\mathcal{J}}$.

In the following, we assume that the number of spline basis functions is roughly equal across different features and use $M := \max_{k,l} \{M_k, O_l\}$ to denote the spline basis in multi-variate splines that uses the most basis functions.

4 Scalable High-order Tensor Product Spline Models

As can be directly inferred from (4), the cost of fitting a bivariate TPS is $\mathcal{O}(p^2 M^2)$. While M is usually kept fixed and of moderate size (e.g., $M = 10$), this implies that models will be increasingly expensive for both a growing number of basis evaluations and number of features p . For models with (up to) D -variate TPS, the computational cost increases to $\mathcal{O}(p^D M^D)$. This makes GAMs infeasible both in terms of computing time and also in terms of memory storage.

4.1 Additive Factorization Machines

To overcome the unfavorable scaling of GAMs with many (or higher-order) TPS, we introduce additive factorization machines (AFMs). Based on the idea of factorization machines, we approximate $f_{k,l}(x_k, x_l)$ in (4) by $\phi_{k,l}(x_k, x_l)$ defined as

$$\sum_{m=1}^{M_k} \sum_{o=1}^{O_l} B_{m,k}(x_k) B_{o,l}(x_l) \sum_{f=1}^F \gamma_{m,k,f} \gamma_{o,l,f}, \quad (8)$$

where $\gamma_{\cdot,k,f} \in \mathbb{R}$ are latent factors approximating the joint effect $\beta_{m,k,o,l}$. When approximating every bivariate interaction term in (4) with the term defined in (8), we can derive the following representation.

Corollary 4.1 (AFM Representation). *The approximation of (8) using (4) can be written as*

$$\sum_{k=1}^p \sum_{l=k+1}^p f_{k,l}(x_k, x_l) \approx \frac{1}{2} \sum_{f=1}^F \left\{ \left[\sum_{k=1}^p \varphi_{k,f} \right]^2 - \sum_{k=1}^p \varphi_{k,f}^2 \right\}, \quad (9)$$

with $\varphi_{k,f} = \sum_{m=1}^{M_k} B_{m,k}(x_k) \gamma_{m,k,f}$.

As a direct result of Corollary 4.1, we obtain the scaling of computing AFMs.

Proposition 4.2 (Linear Scaling of AFMs). *Computations for AFMs scale with $\mathcal{O}(pMF)$.*

Corollary 4.1 and Proposition 4.2 are natural extensions of linearity results from FMs. A proof of the corollary is provided in the Appendix. Roughly speaking, the factorization trick from FMs also works for AFMs in a similar manner as the additional basis function dimension only depends on the respective feature dimension. In particular, this means that AFMs scale linearly both in the number of features p and the spline basis dimension M . Another direct result of this representation and noteworthy property unique to AFMs is given in the following proposition for a dataset of n observations.

Proposition 4.3 (Basis Evaluations in AFMs). *If every feature in AFMs is represented by only one basis, it suffices to evaluate all univariate basis functions once for each feature and the memory costs for storing all features are $\mathcal{O}(npM)$.*

While this seems inconspicuous at first glance, a naïve approach for bivariate models requires storing $\mathcal{O}(np^2M^2)$ entries, which is infeasible if n or p is large. In contrast, AFMs only require the same amount of storage as for a univariate spline model. Note that the number of parameters also (linearly) increases with F and needs to be taken into account for the total required storage. However, Proposition 4.3 specifically looks at the costs of storing basis evaluated features in memory as this can be a storage bottleneck during the pre-processing of GAMs.

4.2 Additive Higher-Order Factorization Machines

We now extend previous results to the general case of a D -variate interaction GAM. By analogy to higher-order FMs Blondel et al. (2015), we refer to our approximation as *additive*

higher-order factorization machines (AHOFMs). The ulterior goal of AHOFMs is to provide a scalable version of a TPS model which includes multivariate splines up to D -variate smooths, i.e.,

$$\eta(\mathbf{x}) = \alpha_0 + \sum_{j=1}^p f_j(x_j) + \sum_{j'>j} f_{j',j}(x_{j'}, x_j) + \dots + \sum_{j_D>\dots>j_1} f_{j_1,\dots,j_D}(x_{j_1}, \dots, x_{j_D}). \quad (10)$$

Assume a TPS representation for all smooth terms in (10) with a maximum number of M basis functions. Then, the cost of computing only the last term in (10) is already $\mathcal{O}(p^D M^D)$ (and analogous for memory costs).

Inspired by Vieta's formula and the ANOVA kernel, we can derive a similar result as given in Blondel et al. (2016) to reduce the cost of computing the d th degree term in AHOFMs. We will make the degree d explicit for γ and φ using the superscript (d) .

Definition 4.4 (Additive Higher-order Term (AHOT)). The f th additive higher-order term (AHOT) of degree $2 \leq d \leq D$ in AHOFMs is given by

$$\Phi_f^{(d)} = \sum_{j_d>\dots>j_1} \prod_{t=1}^d \sum_{m=1}^{M_{j_t}} B_{m,j_t}(x_{j_t}) \gamma_{m,j_t,f}^{(d)}. \quad (11)$$

We use F_d AHOTs to approximate a d -variate smooth:

$$\sum_{f=1}^{F_d} \Phi_f^{(d)} \approx \sum_{j_d>\dots>j_1} f_{j_1,\dots,j_d}(x_{j_1}, \dots, x_{j_d}). \quad (12)$$

and estimate the D -variate TPS model (10) with an AHOFM of degree D , defined as follows.

Definition 4.5 (AHOFM of Degree D). The predictor $\eta(\mathbf{x})$ of an AHOFM of degree D is defined by

$$\alpha_0 + \sum_{j=1}^p B_{m,j}(x_j) \beta_{m,j} + \sum_{d=2}^D \sum_{f=1}^{F_d} \Phi_f^{(d)}. \quad (13)$$

The following corollary defines how to recursively describe all AHOTs for $d \geq 2$ using univariate spline representations $\varphi_{j,f}$ as defined in (9).

Lemma 4.6 (Representation AHOT of Degree d). Let $\Phi_f^{(0)} \equiv 1$ as well as $\Phi_f^{(1)} = \sum_{j=1}^p \varphi_{j,f}^{(d)}$. The degree $d \geq 2$ AHOT can be recursively defined by

$$\Phi_f^{(d)} = \frac{1}{d} \sum_{t=1}^d (-1)^{t+1} \Phi_f^{(d-t)} \left\{ \sum_{j=1}^p [\varphi_{j,f}^{(d)}]^t \right\}. \quad (14)$$

The recursive representation (14) allows us to efficiently calculate AHOTs of higher order. The corresponding proof can be found in the Appendix. As another consequence of this representation, we have the following scaling properties.

Proposition 4.7 (Linear Scaling of AHOFMs). *Computations for AHOFMs scale with $\mathcal{O}(pMFD + \mathcal{F}D^2)$ where $\mathcal{F} = \sum_{d=1}^D F_d$.*

Since D is usually small, computations again roughly scale linear with the number of features, the basis and the latent factor dimension. We also recognize that despite the increased dimension D , every feature basis has to be evaluated only once.

Proposition 4.8 (Basis Evaluations in AHOFMs). *If every feature in AHOFMs is represented by only one basis, it suffices to evaluate all univariate basis functions once for each feature and the memory costs for storing all features are $\mathcal{O}(npM)$.*

While the memory consumption also increases with \mathcal{F} when considering the storage of all γ parameters, Proposition 4.8 again focuses on the storage of all features after applying the basis evaluations. Similar to the kernel trick, higher-order features are not actually calculated and stored in memory, as AHOFMs only work on the (basis evaluated) univariate features independent of D .

In contrast to FMs and HOFMs, AHOFMs require additional considerations to enforce appropriate smoothness of all non-linear functions in (10) without impairing previously derived scaling properties.

4.3 Penalization and Optimization

An additional challenge in learning many, potential high-order TPS, is their optimization in terms of appropriate smoothness.

4.3.1 Penalization

Following the penalization scheme of TPS described in Section 3.2.2, we propose a smoothness penalization for AHOFMs based on the penalties of involved marginal bases $B_{m,j}$ with corresponding difference penalty matrices \mathbf{P}_j . Let $\mathfrak{G}^{(d)}$ be the array of all coefficients

$\gamma_{m,j,f}^{(d)}$ for all $m \in [M], j \in [p], f \in [F_d]$. For simplicity¹, we assume $M_j \equiv M$, so that $\mathfrak{G}^{(d)} \in \mathbb{R}^{M \times p \times F_d}$. Further, let $\mathfrak{G}_{[D]} = \mathfrak{G}^{(1)}, \dots, \mathfrak{G}^{(D)}$ and $\boldsymbol{\gamma}_{j,f}^{(d)} = (\gamma_{1,j,f}^{(d)}, \dots, \gamma_{M,j,f}^{(d)})^\top$, i.e., the Mode-1 (column) fibers of $\mathfrak{G}^{(d)}$, and $\Theta = (\alpha_0, \boldsymbol{\beta}_1, \dots, \boldsymbol{\beta}_p)$.

We define the penalty of AHOFMs as follows.

Definition 4.9 (AHOFM Penalty). The smoothing penalty of AHOFMs is defined as

$$\mathcal{P}(\mathfrak{G}_{[D]}, \Theta) = \sum_{j=1}^p \lambda_j \boldsymbol{\beta}_j^\top \mathbf{P}_j \boldsymbol{\beta}_j + \sum_{d=2}^D \sum_{f=1}^{F_d} \sum_{j=1}^p \lambda_{j,f}^{(d)} \boldsymbol{\gamma}_{j,f}^{(d)\top} \mathbf{P}_j \boldsymbol{\gamma}_{j,f}^{(d)}. \quad (15)$$

Due to the independence assumption of all latent factors involved in every factorization, it is natural to only penalize univariate directions as expressed in Definition 4.9. A regularization that involves multiple dimensions would further result in a non-decomposable penalty w.r.t. the $\boldsymbol{\gamma}_{j,f}^{(d)}$ and make the optimization of AHOFMs more challenging (see Section 4.3.3 for details). The penalized optimization problem for n i.i.d. data points $(y_i, \mathbf{x}_i)_{i \in [n]}$ with $\mathbf{x}_i = (x_{i,1}, \dots, x_{i,p})$ and loss function ℓ is then given by

$$\arg \min_{\mathfrak{G}_{[D]}, \Theta} \sum_{i=1}^n \ell(y_i, \eta_i(\mathbf{x})) + \frac{1}{2} \mathcal{P}(\mathfrak{G}_{[D]}, \Theta). \quad (16)$$

In (16), the smoothing parameters are considered to be tuning parameters. While it is possible in univariate GAMs to estimate the smoothing parameters $\lambda_1, \dots, \lambda_p$ directly, this becomes computational challenging for higher-order TPS due to the exponentially increasing amount of parameters. HOFMs avoid this combinatorial explosion of hyperparameters by setting all the parameters to the same value (Blondel et al., 2016). This, however, is not a meaningful approach for smoothing parameters as every smooth term can potentially live on a completely different domain (e.g., $\lambda = 1$ can imply no penalization for one smooth, but maximum penalization for another smooth term).

4.3.2 Scalable Smoothing

To derive a meaningful penalization in AHOFMs, we exploit the definition of *degrees-of-freedom* for penalized linear smoothers (Buja et al., 1989). Given a matrix of basis

¹Next to a ragged tensor definition that allows for a varying first dimension, padding the tensor can also be an option to always have M dimensions for every feature j .

evaluations $\mathbf{B}_j \in \mathbb{R}^{n \times M_j}$ with entries $B_{m,j}(x_{i,j})$ and a squared penalty matrix \mathbf{P}_j for the penalization of differences in neighboring basis coefficients, there exists a one-to-one map between $\lambda_{j,f}^{(d)}$ and the respective degrees-of-freedom

$$\text{df}_{j,f}^{(d)}(\lambda_{j,f}^{(d)}) = \text{tr}(2\mathbf{H}_j(\lambda_{j,f}^{(d)}) - \mathbf{H}_j(\lambda_{j,f}^{(d)})^\top \mathbf{H}_j(\lambda_{j,f}^{(d)})) \quad (17)$$

with $\mathbf{H}_j(\lambda_{j,f}^{(d)}) = \mathbf{B}_j(\mathbf{B}_j^\top \mathbf{B}_j + \lambda_{j,f}^{(d)} \mathbf{P}_j)^{-1} \mathbf{B}_j^\top$. While the exact degrees-of-freedom only hold for a linear model with a single smooth term, this approach allows to define a meaningful a priori amount of penalization for all smooth terms by restricting their degrees-of-freedom to the same global $\text{df}^{(d)}$ value as follows.

Proposition 4.10 (Homogeneous AHOFM Smoothing). *Given a global $\text{df}^{(d)}$ value, an equal amount of penalization for all $\binom{p}{d}$ AHOTs in $\Phi_f^{(d)}$ is achieved by choosing $\lambda_{j,f}^{(d)}$ such that $\text{df}_{j,f}^{(d)}(\lambda_{j,f}^{(d)}) \equiv \text{df}^{(d)} \forall j \in [p], f \in [F_d]$.*

The Demmler-Reinsch Orthogonalization (DRO; Ruppert et al., 2003) can be used to efficiently solve (17) for $\lambda_{j,f}^{(d)}$, i.e., calculate $\lambda_{j,f}^{(d)}$ based on a given value $\text{df}_{j,f}^{(d)}$. The DRO involves the calculation of singular values \mathbf{s}_j of a squared $M_j \times M_j$ matrix. Once \mathbf{s}_j are computed, (17) can also be solved multiple times for different df values without additional costs (we refer to this step as sv2la). More details are given in Appendix C.1. Moreover, as the factorization only requires univariate smooth terms, $\lambda_{j,f}^{(d)}$ can be calculated for every feature separately at the cost of $\mathcal{O}(M_j^3)$ due to our factorization approach. This computational cost is comparatively small compared to a computation for all features in a D -variate interaction term with $\mathcal{O}(M^{3D})$. Also note that in Proposition 4.10, $\text{df}_{j,f}^{(d)}(\lambda_{j,f}^{(d)})$ only needs to be calculated once for every j as all involved matrices in (17) are independent of f . Another advantage of this approach is that this is a *one-time* computation which can be done prior to the optimization and requires no additional costs during training. Algorithm 1 summarizes the routine. Homogeneous AHOFM smoothing amounts to equally flexible non-linear interactions for every order- d AHOT and hence implies isotropic smoothing for all TPS. Given no a priori information on the non-linear interactions of all features, this is a natural choice. In contrast, if we choose different values for one or more features, i.e., $\exists j : \text{df}_{j,f} \neq \text{df}$, all TPS involving the j th feature are subject to anisotropic smoothing.

Algorithm 1 Homogeneous AHOFM Smoothing

Input: $\mathbf{B}_j, \mathbf{P}_j \forall j \in [p]$; $\text{df}^{(d)} \forall d \in [D]$

for $j = 1$ **to** p **do**

 Compute $\mathbf{s}_j = \text{DRO}(\mathbf{B}_j, \mathbf{P}_j)$ (costs: $\mathcal{O}(M_j^3)$)

for $d = 1$ **to** D **do**

 Compute $\lambda_{j,1}^{(d)} = \text{sv2la}(\mathbf{s}_j, \text{df}^{(d)})$ (negligible costs);

 Set $\lambda_{j,f}^{(d)} = \lambda_{j,1}^{(d)}$ for $f \in [F_d]$;

end for

end for

Output: $\lambda_{j,f}^{(d)}$ for all $j \in [p], d \in [D], f \in [F_d]$

4.3.3 Optimization

Having defined the objective in (16), we obtain the following result.

Lemma 4.11. *The optimization problem in (16) is coordinate-wise convex in $\gamma_{j,f}^{(d)}$.*

A corresponding proof is given in the Appendix. Using this finding, we suggest a block coordinate descent (BCD) solver to optimize (penalized) AHOFMs with block updates for $\gamma_{j,f}^{(d)}$. In contrast to (HO)FMs, we perform block updates instead of plain coordinate descent as the AHOFM penalty is only decomposable w.r.t. all $\gamma_{j,f}^{(d)}$, but not w.r.t. $\gamma_{m,j,f}^{(d)}$. For BCD we require several quantities, which we derive in Appendix C.3. A high-level routine is described in Algorithm 2 (for simplicity for the case with only a single D -variate smooth). In Algorithm 2, we require gradients

$$\nabla \mathcal{L}(\gamma_{j,f}^{(d)}) := \sum_{i=1}^n \frac{\partial \mathcal{L}(\mathbf{x}_i, y_i)}{\partial \gamma_{j,f}^{(d)}},$$

where \mathcal{L} is the objective function from (16) and a learning rate ν , which is defined in Appendix C.3. Various terms involved in the update step can be pre-computed or cached (see Appendix C for details). Using the result in Lemma 4.11, BCD is guaranteed to converge to a stationary point (Bertsekas et al., 1999). In order to scale also for large numbers of observations, an alternative solution are stochastic methods such as a mini-batch gradient descent routine or sub-sampled Newton’s method (see, e.g., Byrd et al., 2011). In practice,

Algorithm 2 BCD AHOFM Optimization

Input: Data $(y_i, \mathbf{x}_i)_{i \in [n]}$; $B_{m,j}, \mathbf{P}_j, \forall j \in [p], m \in [M_j]$; D ; $\text{df}^{(D)}$; F_D ; BCD convergence criterion

Initialization: $\hat{\eta}, \mathfrak{G}^{(D)} = \text{init}(\text{Input})$ (Appendix C.2)

repeat

for $f = 1$ **to** F_D **do**

for $j = 1$ **to** p **do**

 Calculate step-size ν

 Update $\gamma_{j,f}^{(d)} \leftarrow \gamma_{j,f}^{(d)} - \nu \nabla \mathcal{L}(\gamma_{j,f}^{(d)})$

 Synchronize $\hat{\eta}_i, i \in [n]$

end for

end for

until convergence

we noticed very slow convergence of different BCD variants and finding a good choice for hyperparameters in the optimization such as the learning rate proved to be challenging. In contrast, sophisticated stochastic gradient descent routines such as Adam (Kingma and Ba, 2014) showed similar or even better results (for a given limited time budget). We have implemented both these approaches in `TensorFlow` (Abadi et al., 2016) on the basis of the package `deepregression` (Rügamer et al., 2022) to fit additive models in a neural network framework. This allows us to seamlessly change the optimization routine depending on the given data situation and also combine the BCD routine with mini-batch updates.

5 Numerical Experiments

In the following we will investigate the estimation performance (Section 5.1) and scalability (Section 5.2) of AFMs compared to state-of-the-art (SotA) software for fitting large-scale GAMs (Wood, 2011). In addition to the empirical evidence given in these numerical experiments, Section 5.3 presents a benchmark on commonly used benchmarks data sets to compare AFMs against other modeling choices in terms of prediction performance.

5.1 Estimation Performance

We first compare the estimation performance of our proposal with the SotA for fitting GAMs with TPS. More specifically, we simulate features and generate bivariate non-linear effects for every possible feature pair by simulating TPS with $\text{df} \in \{7, 10\}$ degrees-of-freedom in every direction. We then add random noise with a signal-to-noise ratio (SNR) of 0.5 to the sum of all bivariate effects and compare the estimation of these feature effects for both methods. This is done by inspecting the estimated non-linear effects visually, and quantitatively by computing the mean squared error (MSE) between the estimated and true surfaces. For $n \in \{2000, 4000, 8000\}$ and $p = 5$ (resulting in 10 bivariate effects), we run AFMs with $F \in \{1, 3, 5\}$. We repeat every setting 10 times with different random seeds. The GAM estimation can be thought of as a gold standard which is only subject to an estimation error, but no approximation error. In contrast, AFMs are also subject to an approximation error, but might still yield better performance due to the considerably smaller number of parameters that need to be estimated (smaller estimation error). Our quantitative analysis of results confirms this hypothesis. Figure 2 depicts the MSEs for all analyzed settings to compare the estimation performance of AFMs and GAMs when calculating the average point-wise differences between the estimated bivariate surface and the true surface. Results suggest that different numbers of latent dimensions F can be optimal, but, as expected, larger values of F decrease the approximation error. For more complex bivariate effects the GAM is superior as it directly estimates the smoothness while the smoothing parameter for AFMs are kept fixed over all simulations. In cases where $p - 1 \leq F$, the approximation error can theoretically be reduced to zero and the approximation of AFMs tends to yield better results than the GAM (cf. Figure 3 for $p = 3$ and $F = 3$).

5.2 Scalability

Our next experiment investigates the scaling behavior of our approach and compares it to the SotA implementation for big additive models (BAMs Wood et al., 2017). We simulate $p \in \{3, 6, 9, 12\}$ standard normal distributed features for $n \in \{6000, 12000, 18000\}$ observations and fit both BAM and an AFM to learn a GAM with TP splines for all possible

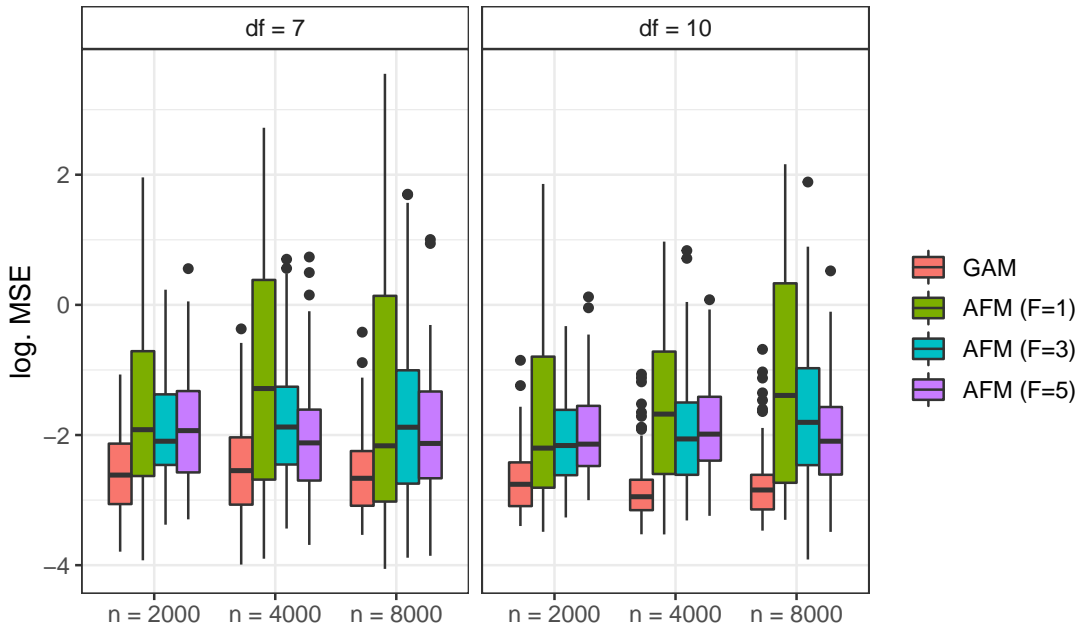


Figure 2: Comparison of the estimation performance (logarithmic MSE) between a GAM implementation (in red) and our proposal with different numbers of latent dimensions F for differently flexible bivariate functions (df value), different numbers of observations (columns), different numbers of features p (x-axis) and observations (columns). Boxplots comprise all 10 bivariate effects and 10 simulation replications.

combinations of the p features. Figure 1 summarizes the results by comparing the memory consumption (in megabyte) and the computing time (in seconds). The results reflect our initial motivation to propose AFMs. While both time and memory consumption grows exponentially in the number of features for BAMs, we observe a linear scaling for AFMs both for the memory consumption and the computation time.

5.3 Benchmark

To also assess the prediction performance of AFMs and AHOFMs, we compare both approaches against a variety of alternatives, namely GAMs with only univariate smooth terms, FMs, HOFMs, and a multilayer perceptron (MLP). As GAMs do not require any

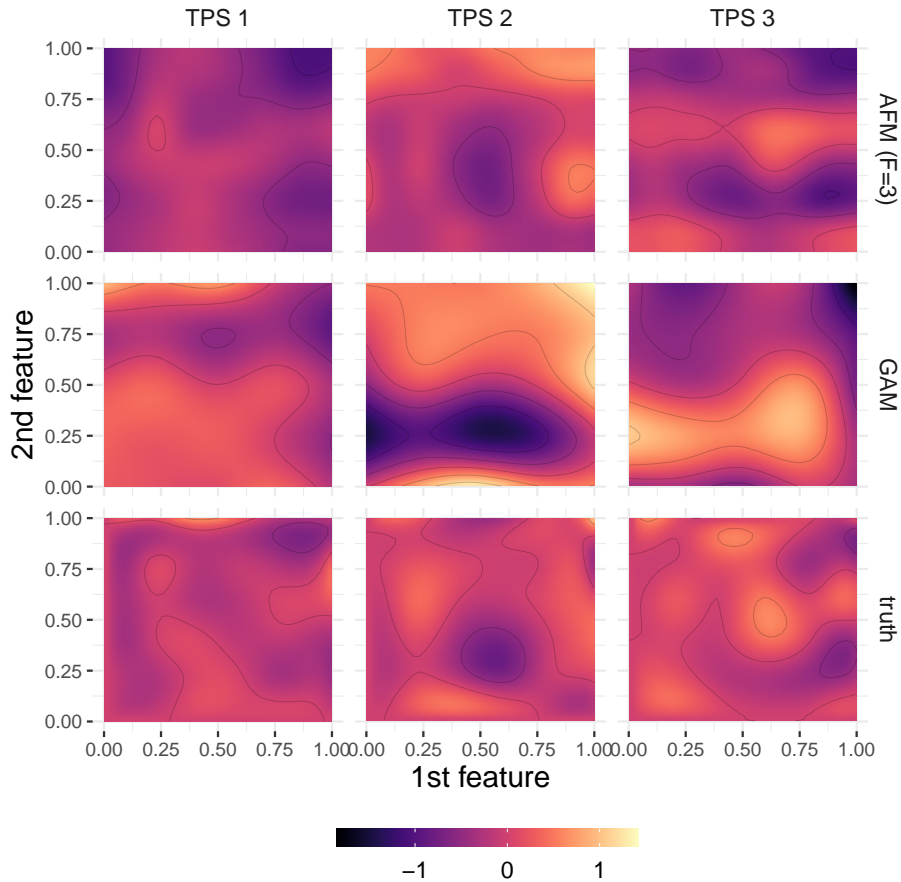


Figure 3: Example ($n = 2000, p = 3$) of estimated and true surfaces visualized by a contour plot for the three TPS (columns). Colours represent the partial effect value. In this case, the AFM provides a better estimation than the GAM.

tuning and all factorization approaches mainly require the number of latent dimensions as tuning parameter (we investigate $F \in \{1, 5, 10\}$), we also only choose between three predefined architectures for the MLP. We compare all methods on commonly used benchmark data sets using 10 train-test splits and report average MSE values as well as their standard deviation. Table 1 summarizes the results when choosing the best performing hyperparameter set per method and data set. Further details on MLP architectures, hyperparameters, the full list of results and details on benchmark data sets can be found in Section F.2 in the Appendix. Results indicate that for many data sets the combination of non-linearity (not provided by FMs and HOFMs) and interactions (not provided by GAMs) of A(HO)FMs

Table 1: Average prediction performances (MSE \downarrow) with standard deviation in brackets for different methods (columns) and benchmark data sets (rows) over 10 different train-test splits. The best method per data set is highlighted in bold, the second best is underlined.

	GAM	FM	HOFM($D = 3$)	MLP	AFM	AHOFM($D = 3$)
Airfoil	119.3 (2.490)	90.70 (45.55)	79.03 (51.29)	4.708 (0.513)	<u>4.314</u> (0.576)	4.181 (0.699)
Concrete	9.768 (8.408)	10.55 (0.970)	10.56 (0.955)	5.648 (0.706)	<u>6.100</u> (0.648)	6.127 (0.491)
Diabetes	142.1 (9.626)	143.7 (10.04)	143.3 (9.312)	<u>57.65</u> (6.597)	57.12 (6.243)	63.65 (9.672)
Energy	3.409 (0.363)	7.487 (0.620)	7.480 (0.632)	3.551 (0.491)	3.137 (0.332)	<u>3.183</u> (0.359)
ForestF	1.465 (0.163)	<u>1.403</u> (0.105)	1.398 (0.107)	1.405 (0.104)	1.573 (0.325)	1.773 (0.307)
Naval	0.002 (0.000)	0.009 (0.001)	0.009 (0.001)	0.004 (0.002)	0.004 (0.002)	<u>0.003</u> (0.001)
Yacht	3.027 (0.517)	8.883 (0.990)	8.898 (0.985)	2.397 (0.614)	<u>2.401</u> (0.618)	1.743 (0.624)

leads to improved predictive performance.

6 Summary and Outlook

In this paper, we presented an additive model extension of HOFMs to allow for scalable high-order smooth function estimation based on tensor product splines. The proposed approach allows fitting GAMs with D -variate smooth terms at costs similar to an univariate GAM. AHOFMs can further improve over the GAM and (HO)FM prediction performance due to the inclusion of interactions and extension to non-linearity. A current limitation of AHOFMs is there quickly growing number of additive effects, making it difficult to interpret the model despite its additive predictor structure. We discuss this issue in Appendix E.

An interesting direction for future research is to view AFMs and AHOFMs through the lens of tensor regression and low-rank approximation as in Blondel et al. (2016). Similar to the extension of HOFMs to AHOFMs, this “lifted” approach (Candes et al., 2015) requires additional consideration. More specifically, as the latent factors $\gamma_{m,j,f}$ vary across two dimensions (m,j) for every f , it is not directly possible to represent $\Phi_f^{(d)}$ as inner product of two rank-one tensors as done in Blondel et al. (2016). We elaborate on possible representations and resulting properties in Appendix D.

SUPPLEMENTARY MATERIAL

Appendix: The appendix includes proofs, algorithmic details as well as further specifications and results of numerical experiments.

Reproducibility: Implemented R package and codes to reproduce the results.

References

- Abadi, M., P. Barham, J. Chen, Z. Chen, A. Davis, J. Dean, M. Devin, S. Ghemawat, G. Irving, M. Isard, et al. (2016). Tensorflow: A system for large-scale machine learning. In *12th {USENIX} symposium on operating systems design and implementation ({OSDI} 16)*, pp. 265–283.
- Adomavicius, G. and A. Tuzhilin (2005). Toward the next generation of recommender systems: A survey of the state-of-the-art and possible extensions. *IEEE transactions on knowledge and data engineering* 17(6), 734–749.
- Baumann, P., T. Hothorn, and D. Rügamer (2021). Deep conditional transformation models. In *Machine Learning and Knowledge Discovery in Databases (ECML-PKDD)*, pp. 3–18. Springer International Publishing.
- Bertsekas, D. P., W. Hager, and O. Mangasarian (1999). Nonlinear programming. athena scientific belmont. *Massachusetts, USA*.
- Blondel, M., A. Fujino, and N. Ueda (2015). Convex factorization machines. In *Joint European Conference on Machine Learning and Knowledge Discovery in Databases*, pp. 19–35. Springer.
- Blondel, M., A. Fujino, N. Ueda, and M. Ishihata (2016). Higher-order factorization machines. In *Advances in Neural Information Processing Systems*, pp. 3351–3359.
- Blondel, M., M. Ishihata, A. Fujino, and N. Ueda (2016). Polynomial networks and factorization machines: New insights and efficient training algorithms. In *International Conference on Machine Learning*, pp. 850–858. PMLR.
- Buja, A., T. Hastie, and R. Tibshirani (1989). Linear Smoothers and Additive Models. *The Annals of Statistics* 17(2), 453 – 510.
- Byrd, R. H., G. M. Chin, W. Neveitt, and J. Nocedal (2011). On the use of stochastic hessian information in optimization methods for machine learning. *SIAM Journal on Optimization* 21(3), 977–995.
- Candes, E. J., Y. C. Eldar, T. Strohmer, and V. Voroninski (2015). Phase retrieval via matrix completion. *SIAM review* 57(2), 225–251.
- Chang, C.-H., R. Caruana, and A. Goldenberg (2021). Node-gam: Neural generalized additive model for interpretable deep learning.

- Chen, H., X. Wang, C. Deng, and H. Huang (2017). Group sparse additive machine. In *Proceedings of the 31st International Conference on Neural Information Processing Systems*, pp. 197–207.
- Chen, Y., P. Ren, Y. Wang, and M. de Rijke (2019). Bayesian personalized feature interaction selection for factorization machines. SIGIR’19, New York, NY, USA, pp. 665–674. Association for Computing Machinery.
- Coraddu, A., L. Oneto, A. Ghio, S. Savio, D. Anguita, and M. Figari (2014). Machine learning approaches for improving condition-based maintenance of naval propulsion plants. *Journal of Engineering for the Maritime Environment*.
- Cortez, P. and A. d. J. R. Morais (2007). A data mining approach to predict forest fires using meteorological data.
- Dua, D. and C. Graff (2017). UCI machine learning repository.
- Eckart, C. and G. Young (1936). The approximation of one matrix by another of lower rank. *Psychometrika* 1(3), 211–218.
- Efron, B., T. Hastie, I. Johnstone, and R. Tibshirani (2004). Least angle regression. *The Annals of statistics* 32(2), 407–499.
- Hastie, T. J. and R. J. Tibshirani (2017). *Generalized additive models*. Routledge.
- Hong, F., D. Huang, and G. Chen (2019). Interaction-aware factorization machines for recommender systems. In *Proceedings of the AAAI Conference on Artificial Intelligence*, Volume 33, pp. 3804–3811.
- Jin, R., D. Li, J. Gao, Z. Liu, L. Chen, and Y. Zhou (2021). Towards a better understanding of linear models for recommendation. In *Proceedings of the 27th ACM SIGKDD Conference on Knowledge Discovery & Data Mining*, KDD ’21, New York, NY, USA, pp. 776–785. Association for Computing Machinery.
- Kingma, D. P. and J. Ba (2014). Adam: A method for stochastic optimization. *arXiv preprint arXiv:1412.6980*.
- Kolda, T. G. and B. W. Bader (2009). Tensor decompositions and applications. *SIAM review* 51(3), 455–500.
- Kopper, P., S. Pölsterl, C. Wachinger, B. Bischl, A. Bender, and D. Rügamer (2021). Semi-structured deep piecewise exponential models. In *Proceedings of AAAI Spring Symposium on Survival Prediction – Algorithms, Challenges, and Applications*, PMLR, pp. 40–53.
- Koren, Y., R. Bell, and C. Volinsky (2009). Matrix factorization techniques for recommender systems. *Computer* 42(8), 30–37.
- Lan, L. and Y. Geng (2019). Accurate and interpretable factorization machines. In *Proceedings of the AAAI Conference on Artificial Intelligence*, Volume 33, pp. 4139–4146.
- Liu, H., L. Wasserman, J. Lafferty, and P. Ravikumar (2008). Spam: Sparse additive models. In J. Platt, D. Koller, Y. Singer, and S. Roweis (Eds.), *Advances in Neural Information Processing Systems*, Volume 20. Curran Associates, Inc.

- Nelder, J. A. and R. W. Wedderburn (1972). Generalized linear models. *Journal of the Royal Statistical Society: Series A (General)* 135(3), 370–384.
- Ortigosa, I., R. Lopez, and J. Garcia (2007). A neural networks approach to residuary resistance of sailing yachts prediction. In *Proceedings of the international conference on marine engineering MARINE*, Volume 2007, pp. 250.
- Pan, D., X. Li, X. Li, and D. Zhu (2020, 7). Explainable recommendation via interpretable feature mapping and evaluation of explainability. In C. Bessiere (Ed.), *Proceedings of the Twenty-Ninth International Joint Conference on Artificial Intelligence, IJCAI-20*, pp. 2690–2696. International Joint Conferences on Artificial Intelligence Organization.
- R Core Team (2021). *R: A Language and Environment for Statistical Computing*. Vienna, Austria: R Foundation for Statistical Computing.
- Rendle, S. (2010). Factorization machines. In *2010 IEEE International conference on data mining*, pp. 995–1000. IEEE.
- Rendle, S., W. Krichene, L. Zhang, and J. Anderson (2020). Neural collaborative filtering vs. matrix factorization revisited. In *Fourteenth ACM Conference on Recommender Systems*, pp. 240–248.
- Rügamer, D., C. Kolb, C. Fritz, F. Pfisterer, P. Kopper, B. Bischl, R. Shen, C. Bukas, L. Barros de Andrade e Sousa, D. Thalmeier, P. Baumann, L. Kook, N. Klein, and C. Müller (2022). deepregression: a flexible neural network framework for semi-structured deep distributional regression. *Journal of Statistical Software*. Accepted.
- Rügamer, D., C. Kolb, and N. Klein (2020). Semi-Structured Deep Distributional Regression: A Combination of Additive Models and Deep Learning. *arXiv preprint arXiv:2002.05777*.
- Ruppert, D., M. Wand, and R. Carroll (2003). *Semiparametric Regression*. Cambridge Series in Statistical and Probabilistic Mathematics. Cambridge University Press.
- Shan, H. and A. Banerjee (2010). Generalized probabilistic matrix factorizations for collaborative filtering. In *2010 IEEE International Conference on Data Mining*, pp. 1025–1030.
- Srebro, N., J. D. Rennie, and T. S. Jaakkola (2004). Maximum-margin matrix factorization. In *NIPS*, Volume 17, pp. 1329–1336. Citeseer.
- Stöcker, A. and S. Greven (2021). Functional additive regression on shape and form manifolds of planar curves. *arXiv preprint arXiv:2109.02624*.
- Tsanas, A. and A. Xifara (2012). Accurate quantitative estimation of energy performance of residential buildings using statistical machine learning tools. *Energy and Buildings* 49, 560–567.
- Wang, Y., H. Chen, F. Zheng, C. Xu, T. Gong, and Y. Chen (2020). Multi-task additive models for robust estimation and automatic structure discovery. In H. Larochelle, M. Ranzato, R. Hadsell, M. F. Balcan, and H. Lin (Eds.), *Advances in Neural Information Processing Systems*, Volume 33, pp. 11744–11755. Curran Associates, Inc.

- Wood, S. N. (2006). Low-rank scale-invariant tensor product smooths for generalized additive mixed models. *Biometrics* 62(4), 1025–1036.
- Wood, S. N. (2011). Fast stable restricted maximum likelihood and marginal likelihood estimation of semiparametric generalized linear models. *Journal of the Royal Statistical Society (B)* 73(1), 3–36.
- Wood, S. N. (2017). *Generalized additive models: an introduction with R*. Chapman and Hall/CRC.
- Wood, S. N., Z. Li, G. Shaddick, and N. H. Augustin (2017). Generalized additive models for gigadata: Modeling the u.k. black smoke network daily data. *Journal of the American Statistical Association* 112(519), 1199–1210.
- Yeh, I.-C. (1998). Modeling of strength of high-performance concrete using artificial neural networks. *Cement and Concrete research* 28(12), 1797–1808.
- Yin, J., X. Chen, and E. P. Xing (2012). Group sparse additive models. In *Proceedings of the... International Conference on Machine Learning. International Conference on Machine Learning*, Volume 2012, pp. 871. NIH Public Access.
- Yuan, F., G. Guo, J. M. Jose, L. Chen, H. Yu, and W. Zhang (2017). Boostfm: Boosted factorization machines for top-n feature-based recommendation. In *Proceedings of the 22nd International Conference on Intelligent User Interfaces, IUI '17*, New York, NY, USA, pp. 45–54. Association for Computing Machinery.
- Zhang, X., Y. Zhou, Y. Ma, B.-C. Chen, L. Zhang, and D. Agarwal (2016). Glmix: Generalized linear mixed models for large-scale response prediction. KDD '16, New York, NY, USA, pp. 363–372. Association for Computing Machinery.
- Zhang, Y., X. Bi, N. Tang, and A. Qu (2021). Dynamic tensor recommender systems. *Journal of Machine Learning Research* 22(65), 1–35.
- Zhou, H., L. Li, and H. Zhu (2013). Tensor regression with applications in neuroimaging data analysis. *Journal of the American Statistical Association* 108(502), 540–552.
- Zhuang, H., X. Wang, M. Bendersky, A. Grushetsky, Y. Wu, P. Mitrichev, E. Sterling, N. Bell, W. Ravina, and H. Qian (2021). Interpretable ranking with generalized additive models. In *Proceedings of the 14th ACM International Conference on Web Search and Data Mining, WSDM '21*, New York, NY, USA, pp. 499–507. Association for Computing Machinery.

A Further Notation and Background

In the following, we use $\langle \cdot, \cdot \rangle$ for the inner product. The inner product between two tensors $\mathfrak{X}, \mathfrak{Y} \in \mathbb{R}^{p_1 \times \dots \times p_D}$ with entries $x_{i_1, \dots, i_D}, y_{i_1, \dots, i_D}$ is given by $\langle \mathfrak{X}, \mathfrak{Y} \rangle = \sum_{i_1, \dots, i_D} x_{i_1, \dots, i_D} y_{i_1, \dots, i_D}$ (see, e.g., Kolda and Bader, 2009). We further define a symmetric rank-one tensor by $\mathbf{a}^{\otimes d} := \underbrace{\mathbf{a} \otimes \dots \otimes \mathbf{a}}_{d \text{ times}}$.

B Proofs

B.1 Proof of Corollary 4.1

$$\begin{aligned}
& \sum_{k=1}^p \sum_{l=k+1}^p \sum_{m=1}^{M_k} \sum_{o=1}^{O_l} B_{m,k}(x_k) B_{o,l}(x_l) \beta_{m,k,o,l} \\
& \approx \sum_{k=1}^p \sum_{l=k+1}^p \sum_{m=1}^{M_k} \sum_{o=1}^{O_l} \sum_{f=1}^F B_{m,k}(x_k) B_{o,l}(x_l) \gamma_{m,k,f} \gamma_{o,l,f} \\
& = \sum_{k=1}^p \sum_{l=k+1}^p \sum_{m=1}^{M_k} \sum_{o=1}^{O_l} \sum_{f=1}^F B_{m,k}(x_k) \gamma_{m,k,f} B_{o,l}(x_l) \gamma_{o,l,f} \\
& = \sum_{f=1}^F \left\{ \sum_{k=1}^p \sum_{m=1}^{M_k} B_{m,k}(x_k) \gamma_{m,k,f} \sum_{l=k+1}^p \sum_{o=1}^{O_l} B_{o,l}(x_l) \gamma_{o,l,f} \right\} \\
& = \sum_{f=1}^F \left\{ \sum_{k=1}^p \sum_{m=1}^{M_k} B_{m,k}(x_k) \gamma_{m,k,f} \sum_{l=k+1}^p \varphi_{l,f} \right\} = \sum_{f=1}^F \left\{ \sum_{k=1}^p \sum_{m=1}^{M_k} \sum_{l=k+1}^p \underbrace{B_{m,k}(x_k) \gamma_{m,k,f}}_{c_{m,k,f}} \varphi_{l,f} \right\} \\
& = \frac{1}{2} \sum_{f=1}^F \left\{ \sum_{k=1}^p \sum_{m=1}^{M_k} \sum_{l=1}^p c_{m,k,f} \varphi_{l,f} - \sum_{k=1}^p \sum_{m=1}^{M_k} c_{m,k,f} \varphi_{k,f} \right\} \\
& = \frac{1}{2} \sum_{f=1}^F \left\{ \left[\sum_{k=1}^p \sum_{m=1}^{M_k} c_{m,k,f} \right] \left[\sum_{l=1}^p \sum_{o=1}^{O_l} c_{o,l,f} \right] - \sum_{k=1}^p \varphi_{k,f}^2 \right\} \\
& = \frac{1}{2} \sum_{f=1}^F \left\{ \left[\sum_{k=1}^p \sum_{m=1}^{M_k} c_{m,k,f} \right]^2 - \sum_{k=1}^p \varphi_{k,f}^2 \right\} \\
& = \frac{1}{2} \sum_{f=1}^F \left\{ \left[\sum_{k=1}^p \varphi_{k,f} \right]^2 - \sum_{k=1}^p \varphi_{k,f}^2 \right\}.
\end{aligned} \tag{18}$$

B.2 Proof of Proposition 4.2 and 4.3

Both propositions directly follow from the fact that (18) only sums over f , k and m once and every basis function $B_{m,k}$ is therefore also only evaluated once.

B.3 Proof of Lemma 4.6

An alternative representation of (4.6) is given by

$$\Phi_f^{(d)} = \sum_{j_d > \dots > j_1} \prod_{t=1}^d \varphi_{j_t, f} \quad (19)$$

by just plugging in the definition for φ . We can consider (19) as an ANOVA kernel of degree d in the new feature space given by all φ s. As a result, the multi-linearity property of the ANOVA kernel holds (see Blondel et al., 2016, Appendix B.1), i.e.,

$$\Phi_f^{(d)} = \Phi_{f, \neg j}^{(d)} + \varphi_{j, f} \Phi_{f, \neg j}^{(d-1)} \quad (20)$$

where $\Phi_{f, \neg j}^{(d)} = \sum_{\{j_d > \dots > j_1\} \setminus j} \prod_{t=1}^d \varphi_{j_t, f}$ and therefore AHOFMs can be represented as in Lemma 4.6 by using the same arguments as for HOFMs (Blondel et al., 2016).

B.4 Proof of Lemma 4.11

For simplicity assume that the model predictor only consists of a single AHOT, i.e., $\eta(\mathbf{x}) = \sum_{f=1}^{F_d} \Phi_f^{(d)}$. The generalization of the following statement to several AHOTs follows due to the additivity of the model predictor.

Using Equation (20) and constants ξ_f, ζ_f , it follows

$$\begin{aligned} \eta(\mathbf{x}) &= \sum_{f=1}^{F_d} \Phi_f^{(d)} = \sum_{f=1}^{F_d} \left\{ \Phi_{f, \neg j}^{(d)} + \varphi_{j, f} \Phi_{f, \neg j}^{(d-1)} \right\} = \sum_{f=1}^{F_d} \{ \xi_f + \varphi_{j, f} \zeta_f \} = \sum_{f=1}^{F_d} \{ \xi_f + \mathbf{B}_j^\top \boldsymbol{\gamma}_{j, f} \zeta_f \} \\ &= \sum_{f=1}^{F_d} \xi_f + (\mathbf{B}_j \otimes \boldsymbol{\zeta})^\top \boldsymbol{\Gamma}_j^{(d)} = \text{const.} + \langle \tilde{\mathbf{B}}_j, \boldsymbol{\Gamma}_j^{(d)} \rangle, \end{aligned} \quad (21)$$

where $\boldsymbol{\Gamma}_j^{(d)} = \text{vec}(\boldsymbol{\mathfrak{G}}_{:,j,:}^{(d)}) \in \mathbb{R}^{MF_d}$, $\tilde{\mathbf{B}} = \mathbf{B}_j \otimes \boldsymbol{\zeta} \in \mathbb{R}^{MF_d}$ and $\boldsymbol{\zeta} = (\zeta_1, \dots, \zeta_{F_d}) \in \mathbb{R}^{F_d}$. (21) shows that η is an affine function in $\boldsymbol{\Gamma}_j^{(d)} \forall j \in [p]$. Now let ℓ be a convex loss function of η

and note that $\mathcal{P}(\mathfrak{G}, \Theta)$ in Definition 4.9 is decomposable across the parameters $\gamma_{j,f}^{(d)}$. The composition of ℓ and η is convex and as \mathcal{P} is decomposable in $\gamma_{j,f}^{(d)}$ and hence also in $\Gamma_j^{(d)}$, the penalized objective in (16) is convex w.r.t. every $\Gamma_j^{(d)}$ and thus every $\gamma_{j,f} \forall j \in [p], f \in [F_d]$.

C Algorithmic Details

C.1 Demmler-Reinsch Orthogonalization

We here describe the DRO (Algorithm 3) and sv2la (Algorithm 4) routine proposed to efficiently compute smoothing penalties. Details can be found in Ruppert et al. (2003), Appendix B.1.1. We use Chol to denote the Cholesky decomposition of a matrix and SVD for the singular value decomposition of a matrix.

Algorithm 3 DRO

Input: Feature matrix $\mathbf{B} \in \mathbb{R}^{n \times M}$, penalty matrix $\mathbf{P} \in \mathbb{R}^{M \times M}$

Compute:

1. $\mathbf{R}^\top \mathbf{R} \leftarrow \text{Chol}(\mathbf{B}^\top \mathbf{B})$
2. $\mathbf{U} \text{diag}(\mathbf{s}) \mathbf{U}^\top \leftarrow \text{SVD}(\mathbf{R}^{-\top} \mathbf{P} \mathbf{R}^{-1})$

Output: singular values \mathbf{s}

Algorithm 4 sv2la

Input: Singular values $\mathbf{s} \in \mathbb{R}^M$, df

Define $\text{dffun}(l) = \sum_{j=1}^M (1 + ls_j)^{-1}$;

Compute: λ for which $\text{dffun}(\lambda) = \text{df}$ using a uniroot search;

Output: λ

C.2 AHOFM Initialization

Algorithm 5 AHOFM Init

Input: Data $(y_i, \mathbf{x}_i), i \in [n]$; order D , bases functions $B_{m,j}, \mathbf{P}_j, j \in [p], m \in [M_j]$; $\text{df}^{(d)}$

Compute the following quantities:

- $\lambda_{j,f}^{(d)} \forall j \in [p], f \in [F_d]$ using Algorithm 1;
- $\nabla \varphi_{j,f}(x_{i,j}) \forall i \in [n]$ as in (22);

Cache the derivatives $\nabla \varphi_{j,f}(x_{i,j})$ for later update steps;

Randomly initialize $\gamma_{j,f}^{(d)}$ and calculate $\varphi_{j,f}^{(d)}$ for all $j \in [p], f \in [F_d]$;

Compute $\hat{\eta}$

Output: $\hat{\eta}, \mathfrak{G}^{(d)}$

C.3 AHOFM Optimization

We can define a Newton-type BCD update for the optimization of AHOFMs. This requires the following quantities:

$$\nabla \varphi_{j,f}(x_{i,j}) := \partial \varphi_{j,f}(x_{i,j}) / \partial \gamma_{j,f} = \mathbf{B}_j(x_{i,j}),$$

$$\begin{aligned} \nabla \Phi_f^{(d)}(\mathbf{x}_i) &:= \frac{\partial \Phi_f^{(d)}(\mathbf{x}_i)}{\partial \gamma_{j,f}^{(d)}} \\ &= \frac{1}{d} \sum_{t=1}^d (-1)^{t+1} \left\{ \frac{\partial \Phi_f^{(d-t)}(\mathbf{x}_i)}{\partial \gamma_{j,f}^{(d)}} \left\{ \sum_{j=1}^p [\varphi_{j,f}^{(d)}(x_{i,j})]^t \right\} + \Phi_f^{(d-t)(\mathbf{x}_i)} \left\{ \sum_{j=1}^p [\varphi_{j,f}^{(d)}(x_{i,j})]^{t-1} \nabla \varphi_{j,f}(x_{i,j}) \right\} \right\}, \end{aligned}$$

$$\nu = \left\{ \sum_{i=1}^n \frac{\partial^2 \ell(\mathbf{x}_i, y_i)}{\partial (\gamma_{j,f}^{(d)})^2} + \lambda_{j,f}^{(d)} \mathbf{P}_j \right\}^{-1}$$

$$\frac{\partial \mathcal{L}(\mathbf{x}_i, y_i)}{\partial \gamma_{j,f}^{(d)}} = \frac{\partial \ell(\mathbf{x}_i, y_i)}{\partial \gamma_{j,f}^{(d)}} \nabla \Phi_f^{(d)}(\mathbf{x}_i) + \lambda_{j,f}^{(d)} \mathbf{P}_j \gamma_{j,f}^{(d)}.$$

(22)

Note that the first term is involved in every update step, but independent of f and the iteration. It is therefore possible to cache the result once at the beginning of the training

routine as also mentioned in Algorithm 5. For reverse-mode differentiation, note that the second term can be calculated efficiently by caching intermediate results.

D Lifted Approach

As the latent factors $\gamma_{m,j,f}$ vary across two dimensions (m,j) for every f , it is not directly possible to represent $\Phi_f^{(d)}$ as inner product of two rank-one tensors as done in Blondel et al. (2016). We can, however, define the following inner product notation

$$\langle \mathfrak{X}, \mathfrak{Y} \rangle_{>M} = \sum_{j_1, \dots, j_d \in \mathcal{M}} x_{j_1, \dots, j_d} y_{j_1, \dots, j_d}$$

with $\mathcal{M} = \{j_1, \dots, j_d : j_i = j_i + M_{j_{i-1}} \forall i \in \{2, \dots, d\}\}$ and represent $\Phi_f^{(d)}$ as

$$\Phi_f^{(d)} = \langle \mathbf{g}^{\otimes d}, \mathbf{b}^{\otimes d} \rangle_{>M}, \quad (23)$$

where $\mathbf{g} = \text{vec}(\mathfrak{G}_{:::,f}^{(d)})$ are the stacked $\gamma_{m,j,f}$ values and $\mathbf{b} = (B_{1,1}, \dots, B_{M,p,p}) \in \mathbb{R}^{\sum_j M_j}$ the stacked $B_{m,j}(x_j)$ values. A more concise formulation can be obtained when directly working with the univariate splines φ :

$$\Phi_f^{(d)} = \frac{1}{2} \langle \boldsymbol{\varphi}_f^{\otimes d}, \mathbf{1}_p^{\otimes d} \rangle_{>0}$$

with $\boldsymbol{\varphi}_f = (\varphi_{1,f}, \dots, \varphi_{p,f}) \in \mathbb{R}^p$ and $\mathbf{1}_p$ a vector of p ones. As a consequence of (23), Lemma 6 from Blondel et al. (2016) applies, which implies that we can make use of the same symmetrization operation to derive a multi-convex formulation.

E Interpretability of A(HO)FMs

Due to their additivity assumption, every additive feature effect in GAMs can be interpreted on its own (*ceteris paribus*). Although AHOFMs inherit some of the interpretability properties from GAMs, e.g., their additivity, interpreting higher-order (non-linear) interaction terms remains challenging and cannot be done without considering lower-order effects of the same feature. For larger values of p , the quickly growing number of additive terms further makes it infeasible to grasp the influence of certain features or interactions. While this is a

limitation of the current approach, we here propose two ways to check effects for models with small to moderate p . The first approach examines interaction terms by visualizing the single univariate smooth terms $\varphi_{j,f}^d$ for $f = 1, \dots, F^d$ and all involved feature dimensions j . Analyzing the univariate latent dimensions separately is not a new approach and the use of factorization approaches can even be motivated by the need to interpret higher-dimensional interactions in lower dimensions. This practice is also used for additive models (see, e.g., Stöcker and Greven, 2021) when smooth effects go beyond two dimensions. An advantage of the analysis of univariate directions is its straightforward combination with univariate effects from lower-order terms. Another approach which focuses only on the interaction effects itself is to visualize the actual approximations ϕ_{j_1, \dots, j_d} as defined in (8). This reduces the number of terms to analyze by the factor F_d , but requires a method for presenting the d -variate effect. As shown in Figure 4, one approach is to visualize the marginals of these multivariate functions together with their variation across the respective other dimensions.

Experiments To demonstrate these approaches, we simulate a toy example for $D = 3$ with four features. For better understanding the features are referred to as *time*, *lat*, *lon* and *rate*. The outcome is assumed to be normally distributed with $\sigma = 0.1$ and the mean given by the sum of all possible smooth 3-way interactions of the features. To simulate non-linear three-dimensional functions, we use a basis evaluation of features with 4 degrees-of-freedom for *time*, 5 degrees-of-freedom for *lat*, 7 degrees-of-freedom for *lon* and 5 degrees-of-freedom for *rate*. Partial effects for each three-dimensional smooth are generated by calculating the TP for these basis and randomly drawing coefficients for the resulting TPS. We generate 10^4 observations, fit a AHOFM($D = 3$) and visualize the resulting effects in two different ways. One approach, as described above is to look at the smooth effects in all F_d latent dimensions. Another approach to interpret effects is to compute the actual approximation ϕ_{j_1, \dots, j_d} as defined in (8) and plot their marginal univariate effects against each feature j_1, \dots, j_d . Figure 4 depicts this idea by plotting the marginal univariate effects of all the four features for all four 3-way interaction effects. This allows us to see how each feature marginally affects each of the interaction terms. Additionally, Figure 4 shows how much variation the marginal effects have in the respective other two dimensions and thereby provides

information on how much the features interact with the respective two other variables. In Figure 5 we visualize the univariate spline factors estimated for the above model. The corresponding three-dimensional effects that were actually estimated can be obtained by multiplying the three respective univariate splines across the same factor dimension.

F Further Results and Details

F.1 Numerical Experiments

F.1.1 Further Results

Comparison Figure 6 shows another example of estimated surfaces similar to Figure 3.

F.2 Benchmark

F.2.1 Implementation

A fair comparison between the different methods in our benchmark is not straightforward, for example, as there are different basis function definitions in different programming languages. In order to make a fair comparison between the different methods, we implement all methods in TensorFlow (Abadi et al., 2016) and R (R Core Team, 2021) to avoid differences in performance due to different software implementations.

F.2.2 Hyperparameter Sets

As described in Section 5.3, neither GAMs, (HO)FMs nor AHOFMs have many hyperparameters to tune. We investigate the influence of the latent dimension by testing $F = 1, 5, 10$ for all approaches and, for a fair comparison between GAMs and A(HO)FMs, set the df values for all methods to the same value 15. For the MLP, we define three 3-layer architectures with 0.1 dropout rate after each of the two hidden layers. Hidden layers are defined using a ReLU activation, the output layer using no activation (due to the regression objective). The three different architecture then differ in their number of units with the options a)

Table 2: Data set characteristics, additional pre-processing and references.

Dataset	# Obs.	# Feat.	Pre-processing	Reference
Airfoil	1503	5	-	Dua and Graff (2017)
Concrete	1030	8	-	Yeh (1998)
Diabetes	442	10	-	Efron et al. (2004)
Energy	768	8	-	Tsanas and Xifara (2012)
ForestF	517	12	logp1 transformation for <code>area</code> ; numerical representation for <code>month</code> and <code>day</code>	Cortez and Morais (2007)
Naval	11934	16	-	Coraddu et al. (2014)
Yacht	308	6	-	Ortigosa et al. (2007); Dua and Graff (2017)

16/4/1, b) 100/10/1 and c) 20/20/1. All methods use early stopping on 10% validation data with a patience of 50.

F.2.3 Benchmark Data Sets

Table 2 lists the data characteristics and pre-processing steps for our benchmark data. The Table 3 shows the results for all models fitted in the benchmark.

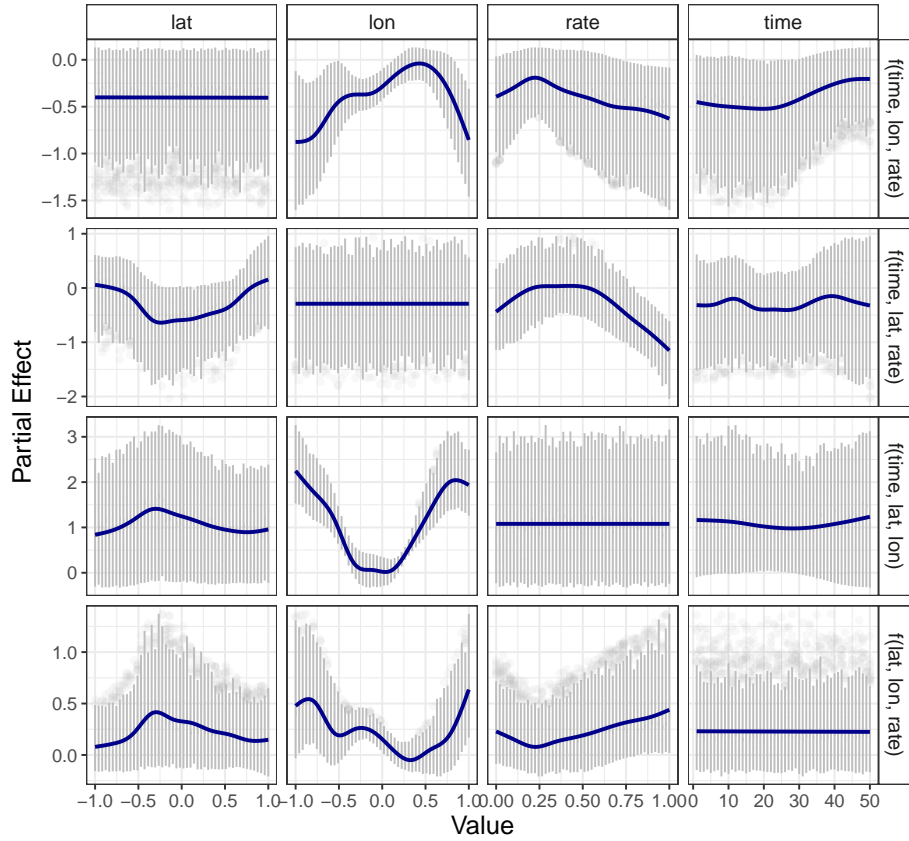


Figure 4: Estimated partial effects of different features (columns) for different three-dimensional functions (rows). Blue lines indicate the marginal average in the respective feature direction while gray vertical lines show the spread across the other two dimensions. More variation indicates larger variation across the other two dimensions. Features not involved in a partial effect (diagonal from top left to bottom right) naturally have a constant effect.

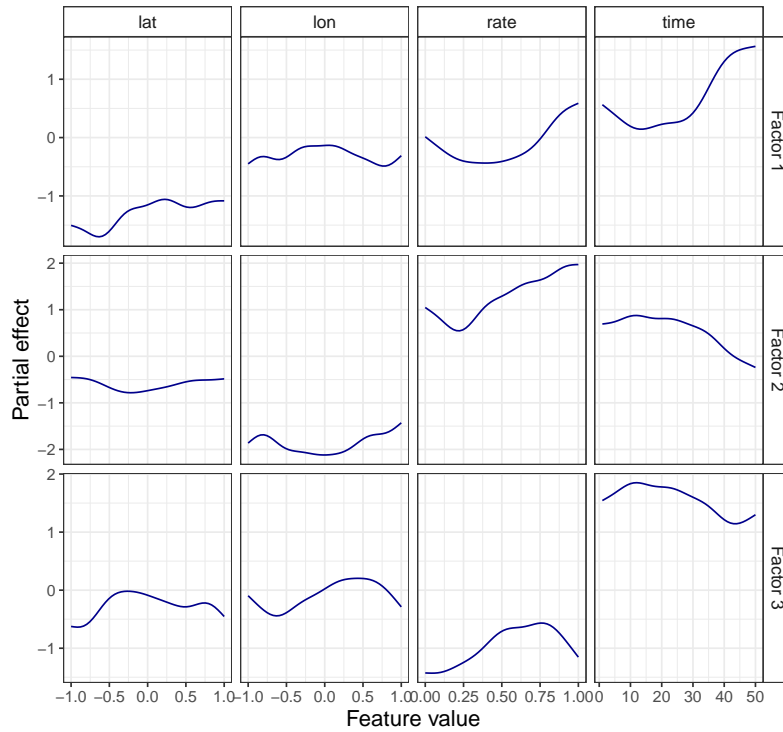


Figure 5: Univariate latent splines estimated for the three-dimensional TPS with marginal effects in Figure 4. Three-dimensional effects can be obtained by multiplying the three respective univariate splines across the same factor dimension.

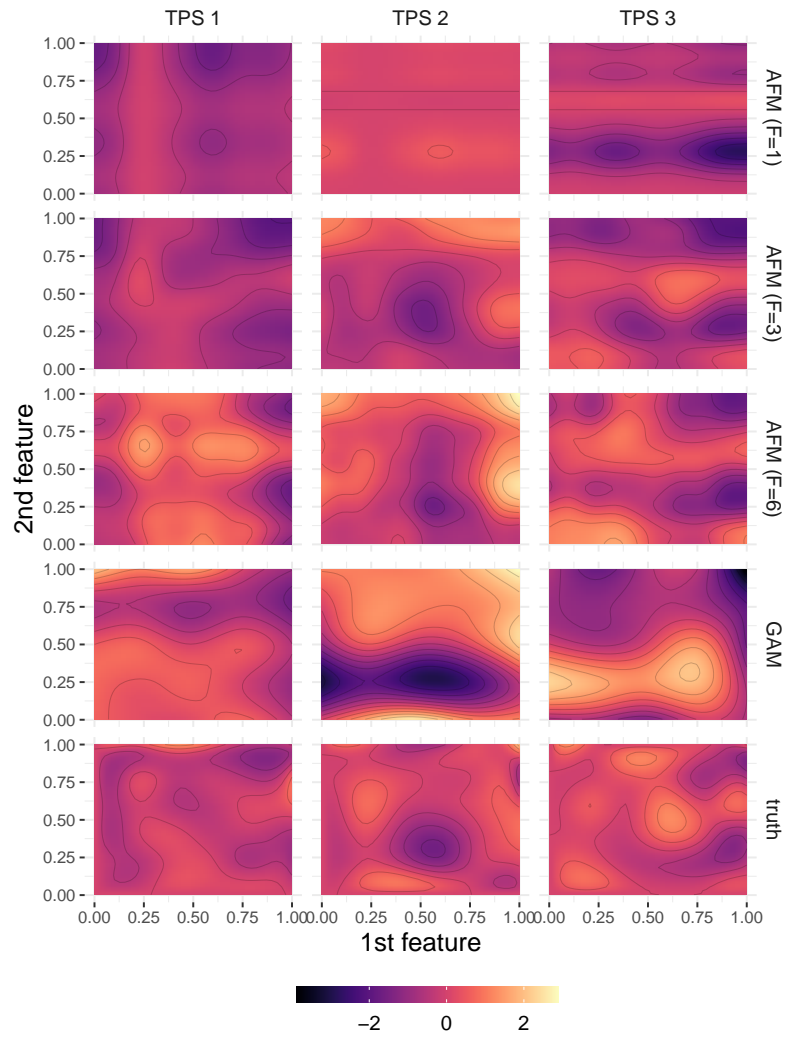


Figure 6: Example ($n = 2000$, $p = 3$) of estimated and true surfaces visualized by a contour plot for the three TPS (columns) based on different models (rows).

Table 3: Average prediction performances (MSE \downarrow) with standard deviation in brackets for different methods (columns) and benchmark data sets (rows) over 10 different train-test splits.

	Airfoil	Concrete	Diabetes	Energy	ForestF	Naval	Yacht
GAM	119.3 (2.49)	9.768 (8.408)	142.1 (9.626)	3.409 (0.3626)	1.465 (0.1632)	0.002391 (0.0004268)	3.027 (0.5174)
FM($F = 1$)	99.61 (40.02)	10.57 (0.9486)	143.8 (7.824)	7.487 (0.6197)	1.424 (0.09161)	0.009454 (0.0009056)	9.056 (1.121)
FM($F = 5$)	108.4 (31.38)	10.56 (0.9808)	143.7 (10.04)	7.496 (0.6215)	1.403 (0.1047)	0.009499 (0.001062)	9.013 (1.174)
FM($F = 10$)	90.7 (45.55)	10.55 (0.9697)	145.6 (8.753)	7.497 (0.6323)	1.444 (0.07558)	0.01017 (0.001775)	8.883 (0.9903)
HOFM($D = 3, F = 1$)	99.14 (39.73)	10.56 (0.9546)	145 (7.012)	7.491 (0.607)	1.416 (0.09707)	0.009527 (0.001084)	9.048 (1.191)
HOFM($D = 3, F = 5$)	79.03 (51.29)	13.06 (7.791)	143.3 (9.312)	7.483 (0.6208)	1.398 (0.1065)	0.009469 (0.001104)	8.898 (0.9845)
HOFM($D = 3, F = 10$)	90.33 (45.24)	10.57 (0.9577)	144.3 (9.936)	7.48 (0.6322)	1.425 (0.09739)	0.00945 (0.0008136)	8.919 (0.9584)
MLP (a)	5.107 (0.4068)	8.979 (2.488)	61.16 (8.734)	4.603 (1.08)	1.405 (0.104)	0.008126 (0.004298)	4.19 (1.106)
MLP (b)	4.708 (0.5131)	5.648 (0.7057)	61.54 (8.454)	3.608 (0.4784)	1.447 (0.1095)	0.004887 (0.003593)	2.397 (0.6142)
MLP (c)	5.377 (0.8983)	6.559 (0.7125)	57.65 (6.597)	3.551 (0.4912)	1.426 (0.1174)	0.004064 (0.001554)	2.817 (0.5783)
AFM($F = 1$)	6.257 (0.6817)	6.86 (0.8062)	57.12 (6.243)	3.252 (0.3928)	1.573 (0.3246)	0.004172 (0.002472)	2.72 (0.424)
AFM($F = 5$)	5.054 (0.6354)	6.1 (0.6481)	63.38 (8.439)	3.16 (0.3255)	2.213 (0.6887)	0.005129 (0.001149)	2.401 (0.6176)
AFM($F = 10$)	4.314 (0.576)	6.394 (0.6057)	71.25 (11)	3.137 (0.3317)	2.744 (0.8303)	0.006061 (0.002168)	2.478 (0.4912)
AHOFM($D = 3, F = 1$)	6.13 (1.128)	6.127 (0.4907)	63.65 (9.672)	3.183 (0.3592)	1.733 (0.307)	0.003169 (0.000632)	2.294 (0.8019)
AHOFM($D = 3, F = 5$)	7.922 (4.093)	6.792 (1.015)	245.8 (287)	3.213 (0.3262)	80.66 (155.6)	0.005347 (0.002592)	1.743 (0.6235)
AHOFM($D = 3, F = 10$)	4.181 (0.699)	6.935 (1.612)	185.1 (122.4)	3.333 (0.4464)	59.06 (71.98)	0.006168 (0.002397)	3.033 (3.921)